International Journal of Minerals, Metallurgy and Materials
Volume 30, Number 6, June 2023, Page 1207
https://doi.org/10.1007/s12613-022-2489-1

Effects of ZnO, FeO and Fe_2O_3 on the spinel formation, microstructure and physicochemical properties of augite-based glass ceramics

Shuai Zhang, Yanling Zhang✉, *and Shaowen Wu*

State Key Laboratory of Advanced Metallurgy, University of Science and Technology Beijing, Beijing 100083, China
(Received: 15 January 2022; revised: 30 March 2022; accepted: 31 March 2022)

Abstract: Augite-based glass ceramics were synthesised using ZnO, FeO, and Fe_2O_3 as additives, and the spinel formation, matrix structure, crystallisation thermodynamics, and physicochemical properties were investigated. The results showed that oxides resulted in numerous preliminary spinels in the glass matrix. FeO, ZnO, and Fe_2O_3 influenced the formation of spinel, while FeO simplified the glass network. FeO and ZnO promoted bulk crystallisation of the parent glass. After adding oxides, the grains of augite phase were refined, and the relative quantities of augite crystal planes were also influenced. All samples displayed good mechanical properties and chemical stability. The 2wt% ZnO-doping sample displayed the maximum flexural strength (170.3 MPa). Chromium leaching amount values of all the samples were less than the national standard (1.5 mg/L), confirming the safety of the materials. In conclusion, an appropriate amount of zinc-containing raw material is beneficial for the preparation of augite-based glass ceramics.

Keywords: spinel; network structure; thermodynamics; microstructure; glass ceramics

1. Introduction

During the production of glass ceramics, sometimes a nucleating agent is added into the glass matrix to promote bulk crystallisation in the subsequent heat treatment process [1–5]. This results in the formation of many main crystal phase grains in the matrix, with uniform distribution and similar sizes.

Cr_2O_3, an excellent nucleating agent, is widely used for studying the preparation of glass ceramics [6–9]. On one hand, Cr^{3+} ion has a large field strength that attracts other small atoms during the crystallisation process. Hence, adding a small amount of Cr_2O_3 has a very significant effect on the grain refinement [10]. On the other hand, the spinel phase formed by Cr_2O_3 can be regarded as a heterogeneous nucleating agent, which provides an interface for the crystal growth and promotes bulk crystallisation.

In the previous studies, epitaxial growth phenomenon was observed between the spinel and pyroxene phases, which indicated that the spinel phase, because of its structure, could be an excellent nucleating agent in the preparation of pyroxene-based glass ceramics [11]. At the same time, in the author's previous research, it was determined that after the heat treatment of the parent glass doped with 1.5wt% Cr_2O_3 and 3.5wt% CaF_2, spinel and pyroxene formed a microstructure with spinel as the core and surrounded by the pyroxene phase, and displayed the best physical and chemical properties in the experimental group [12]. The advantage of this structural group is that the interlacing phenomenon of pyroxene phase can be promoted, thus enhancing the strength and performance.

To realize this structure, it is necessary to perform a detailed investigation of the uniform formation and distribution of the spinel phase in the glass matrix. Cr_2O_3 tends to combine with other oxides, such as ZnO, FeO and Fe_2O_3, to form a spinel phase with an AB_2O_4 structure, wherein Zn^{2+} and Fe^{2+} ions occupy position A and Fe^{3+} ions occupy position B [13–14]. The lattice parameters of the spinel are modified to a certain degree, through the formation of solid structures with other oxides. The number and size of spinel in the glass matrix are also influenced. These factors collectively affect the orientation growth of pyroxene. However, the effects of these oxides on the formation of spinel in the matrix, microstructure, and properties of glass ceramics after heat treatment were not fully researched. Therefore, considering crystallisation kinetics and thermodynamics, this study explored the influence of ZnO, FeO, and Fe_2O_3 on the spinel core in pyroxene-based glass ceramics from different aspects, and at the same time, the physical and chemical properties were also measured and analysed. With the development of Chinese industries, a large amount of solid waste containing heavy metals has been produced. For utilizing the Fe and Zn containing waste and resource, we believe that this study provides more insights on the production of glass ceramics materials.

✉ Corresponding author: Yanling Zhang E-mail: zhangyanling@metall.ustb.edu.cn

2. Experimental

2.1. Sample preparation

In this experiment, the glass ceramics were synthesised by two-step melting method. The raw materials were mixed according to Table 1. Extra 1wt%–2wt% of FeO/Fe_2O_3/ZnO was added in the glass matrix. The reagents used in this research were analytical grade and obtained from Sinopharm Chemical Reagent Co., Ltd (China). After drying at 1000°C for 10 h to remove the moisture and volatiles, the mixed raw materials were placed into a corundum crucible, and heated in a horizontal furnace (BLMT-GA, China) with a heating rate 5°C/min to a target temperature of 1500°C. The heating process was maintained in an Ar environment. After melting for 1 h, the melted liquid was poured into a preheated graphite mold and annealed at 600°C for 1 h to obtain the parent glass. According to the thermal analysis curve, nucleation and crystallization temperatures were obtained for setting heat treatment. The contents of Fe in bivalent and trivalent states of parent glass were measured by chemical analysis method (Table 2). The results show that Fe in bivalent state dominates in the FeO-doping sample, while Fe in trivalent state dominates in the Fe_2O_3-doping sample.

Part of the parent glass was sampled and ground to 200 mesh for observation of the glass matrix and subsequent structural analysis, while the rest was heat-treated. After being polished and etched by a 10wt% HF solution for 30 s, the heat-treated samples were sampled and sprayed with gold for microstructure observations and semi-quantitative element analyses.

Table 1. Chemical composition of samples wt%

Sample	Glass matrix							Additive		
	CaO	MgO	Al_2O_3	SiO_2	Na_2CO_3	Cr_2O_3	CaF_2	Fe_2O_3	ZnO	FeO
1Fe_2O_3	14.85	14.85	9.90	49.50	4.95	1.49	3.47	0.99	—	—
2Fe_2O_3	14.71	14.71	9.80	49.02	4.90	1.47	3.43	1.96	—	—
1ZnO	14.85	14.85	9.90	49.50	4.95	1.49	3.47	—	0.99	—
2ZnO	14.71	14.71	9.80	49.02	4.90	1.47	3.43	—	1.96	—
1FeO	14.85	14.85	9.90	49.50	4.95	1.49	3.47	—	—	0.99
2FeO	14.71	14.71	9.80	49.02	4.90	1.47	3.43	—	—	1.96

Table 2. Contents of Fe^{2+} and Fe^{3+} in Fe containing samples wt%

Fe ion form	1FeO	2FeO	1Fe_2O_3	2Fe_2O_3
Fe^{2+}	63.5	70.5	44.9	42.5
Fe^{3+}	36.5	29.5	55.1	57.5

2.2. Characterization and measurement

The mineral phases of both the parent glass and glass ceramics were characterized by X-ray diffraction (XRD; Rigaku, Cu K_α, 10°–90°, Japan). The network structure and chemical bonds of the parent glass and spinel were measured using Raman spectrometer (HORIBA, LabRAM HR Evolution, Japan). The measurements were kept at room temperature 25°C within the wavelength range of 100–2000 cm^{-1}. Differential scanning calorimeter (DSC; Mettler-Toledo, DSC 3+, Switzerland) was used to analyze the thermal phenomenon of parent glass during heating process at the heating rates of 5, 10, 15, and 20°C/min (temperature range: 20–1000°C). Scanning electron microscope microscopy (FEI, MLA250, SEM, America) was used for observing the microstructure of the glass ceramics. The chemical composition of the mineral phase was determined by quantitative analysis using an electron microprobe (SHIMADZU, EPMA-1600, EPMA, Japan).

Based on Archimedes' method, the density of the glass ceramics samples was calculated using the following equation:

$$\rho_{gc} = \frac{M_{gc}}{M_{gc} - M_w} \quad (1)$$

where ρ_{gc} is the density of the glass ceramics, M_{gc} is the mass of the glass ceramics, and M_w represents the mass of overflowing water. The flexural strengths were tested by a three-point bending method using a universal testing machine (Zwick GmbH, Zwick Z010, Germany). According to GB/T 6569-2006 standard, the glass ceramics were cut into strip-shaped samples with dimensions of 3 mm × 4 mm × 40 mm. For each group, the average value of three samples was taken. The flexural strength was calculated by the following equation:

$$\sigma_f = \frac{3FL}{2bd^2} \quad (2)$$

where σ_f (MPa) is the flexural strength of the sample, F (N) stands for the maximum load, L (mm) stands for the span of the sample, and b (mm) and d (mm) represent the width and height of the sample respectively.

According to HJ 557-2010 national standard, the Cr leaching amount was measured by the horizontal vibration method using a liquid/solid ratio of 10 L/kg. During measurement process, the sample was vibrated and allowed to stand for 8 and 16 h respectively. The leaching mixture was filtered through microporous membrane to obtain the leachate, which was stored in a dark place. Based on JC/T 2138-2012 standard, the acid and alkali resistances of glass ceramics were measured by using H_2SO_4 (3 mol/L) and NaOH (6 mol/L) solutions. The chemical stability (K) was calculated by the weights of sample before corrosion (m) and

after corrosion (m_1) using the following equation:

$$K = \frac{m_1}{m} \times 100\% \quad (3)$$

3. Results and discussion

3.1. Effect of oxides on the matrix structure and formation of spinel

The XRD diffraction peaks of the parent glass are shown in Fig. 1. No obvious diffraction peak was observed in the mineral phase of the sample containing FeO. By contrast, the diffraction peaks were observed in the spinel phase after the addition of ZnO and Fe_2O_3. Zhao *et al.* [15] found that a small amount of preliminary spinel appeared in the matrix during the cooling process. The addition of Fe_2O_3 significantly increased the peak intensity of the Cr-spinel, indicating that Fe_2O_3 can promote the formation of spinel in the matrix.

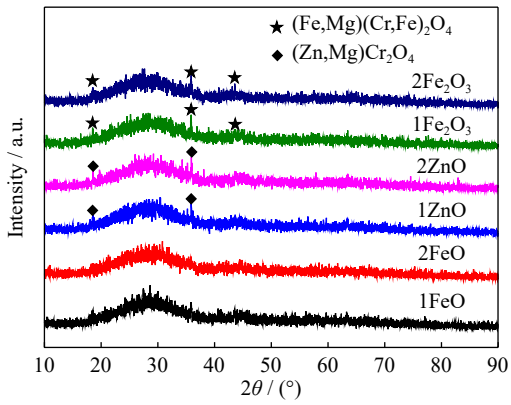

Fig. 1. XRD patterns of the parent glass samples.

Fig. 2 shows the microstructures of the parent glass samples. Small amounts of spinel with different sizes and shapes can be observed in the matrix. The spinel sizes in the samples containing FeO and Fe_2O_3 were relatively larger (FeO: 2.60–4.38 μm; Fe_2O_3: 1.72–2.29 μm), and the spinels were primarily in an irregular multilateral shape. This result was similar with that of Li *et al.* [16]. The addition of FeO increased the number and size of spinel phase.

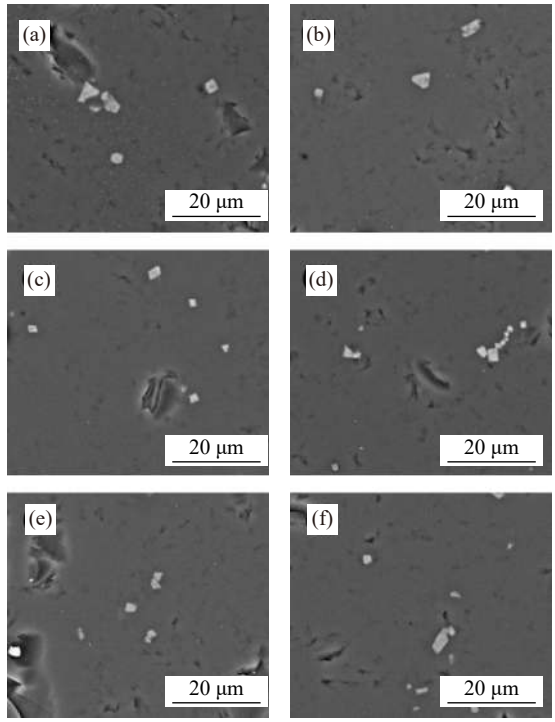

Fig. 2. Microstructure of the parent glass samples: (a) 1FeO; (b) 2FeO; (c) 1ZnO; (d) 2ZnO; (e) $1Fe_2O_3$; (f) $2Fe_2O_3$.

By contrast, the spinel of ZnO-doping sample had a smaller size (ZnO: 1.22–1.93 μm) and a more regular shape, predominantly similar to a parallelogram. Combined with the XRD data analysis, it was determined that although spinel with a large size formed locally in glass matrix, FeO would inhibit the formation of preliminary spinel. Furthermore, the addition of ZnO and Fe_2O_3 resulted in a large number of preliminary spinel with relatively small size in the matrix.

Table 3 lists the electron probe X-ray microanalyser (EPMA) data of the glass matrix and spinel. The results show that certain amounts of Fe^{2+}, Fe^{3+}, and Zn^{2+} ions were soluble in the structure of spinel, while the order of solid solution ratio of elements was $Zn^{2+} > Fe^{2+} > Fe^{3+}$. Furthermore, the addition of FeO increased the content of chromium in the matrix, while the addition of Fe_2O_3 had the opposite effect. This may

Table 3. EPMA quantitative analysis of parent glass mol%

Sample	Phase	Composition (Relative error)						
		CaO (2%)	MgO (2%)	Al_2O_3 (2%)	SiO_2 (2%)	Cr_2O_3 (5%)	ZnO (5%)	FeO (5%)
1FeO	Matrix	19.477	21.455	6.343	51.011	0.232	—	1.482
	Spinel	1.658	43.338	6.468	3.285	40.425	—	4.826
2FeO	Matrix	18.977	20.689	6.033	51.084	0.316	—	2.899
	Spinel	1.383	44.419	5.937	4.962	37.625	—	9.649
1ZnO	Matrix	18.005	21.887	6.334	52.899	0.168	0.686	—
	Spinel	1.415	41.022	7.188	0.876	42.983	6.516	—
2ZnO	Matrix	19.037	22.087	6.366	50.762	0.171	1.577	—
	Spinel	1.442	37.275	8.047	1.159	41.682	10.394	—
$1Fe_2O_3$	Matrix	19.832	21.509	6.105	51.082	0.328	—	1.135
	Spinel	2.883	42.661	6.482	8.696	35.489	—	3.788
$2Fe_2O_3$	Matrix	19.665	21.257	6.606	50.002	0.292	—	2.177
	Spinel	3.950	40.725	6.779	8.410	34.129	—	6.007

be due to the generation of substantial amounts of preliminary spinel in Fe_2O_3-doping sample.

In silicon aluminum oxygen network structure, Q^mSi and Q^mAl represent the connection mode of silicon oxygen tetrahedron [SiO_4] and aluminum oxygen tetrahedron [AlO_4], respectively. Based on previous studies, the characteristic frequencies of 880, 900, 950, 1050, and 1150 cm^{-1} represent Q^0Si (monomer), Q^1Si (dimer), Q^2Si (chain), Q^3Si (sheet), and Q^4Si (net), respectively, and 730, 780 and 850 cm^{-1} represent Q^2Al (chain), Q^3Al (sheet), and Q^4Al (net), respectively [17–19], while 690 cm^{-1} represents the symmetrical stretching vibration of CrO_6. Fig. 3 shows the Raman spectra of the parent glass in the range of 650–1200 cm^{-1}. Through Gaussian peak differentiation [20], the area proportion of the fitting peak was positively correlated with its relative content in the glass matrix. The relative content fraction of the structure unit Q^mSi can then be calculated using the equation [21]:

$$C_{Q^m\mathrm{Si}} = \frac{A_{Q^m\mathrm{Si}}}{(A_{Q^1\mathrm{Si}} + A_{Q^2\mathrm{Si}} + A_{Q^3\mathrm{Si}} + A_{Q^4\mathrm{Si}} + A_{Q^0\mathrm{Si}})} \times 100\% \quad (4)$$

where $C_{Q^m\mathrm{Si}}$ represents the relative content fraction of the structure unit Q^mSi, and $A_{Q^m\mathrm{Si}}$ is the area ratio of its characteristic peak. Table 4 lists the calculation results.

The results showed that with the addition of oxides, the proportion of structural units in the glass matrix did not change much, while the content of Q^3Si unit of the FeO-doping sample was relatively less. Oppositely, FeO was more likely to inhibit the formation of spinel and influence the structure of parent glass, which led to the enrichment of Cr elements in glass matrix. A previous study found that the addition of FeO can effectively reduce the viscosity of the melt

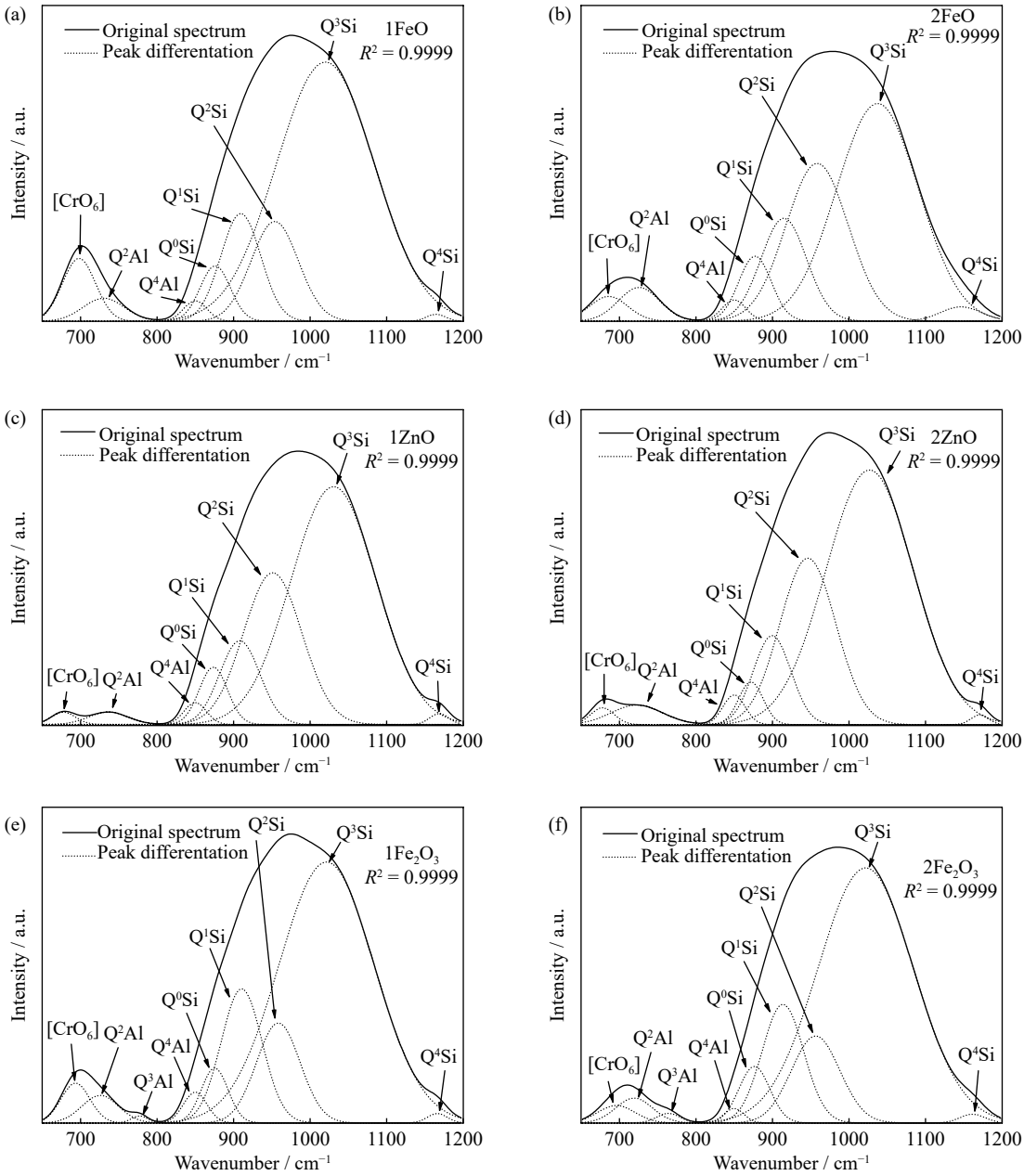

Fig. 3. Peak differentiations in the Raman spectra of the parent glass (range of 650–1200 cm^{-1}): (a) 1FeO; (b) 2FeO; (c) 1ZnO; (d) 2ZnO; (e) 1Fe_2O_3; (f) 2Fe_2O_3.

Table 4. Structural unit content of the parent glass within $R^2 > 0.9999$ %

Sample	Q^0Si (SiO_4^{4-})	Q^1Si ($Si_2O_7^{6-}$)	Q^2Si ($Si_2O_6^{4-}$)	Q^3Si ($Si_2O_5^{2-}$)	Q^4Si (SiO_4)
$1Fe_2O_3$	4.52	10.78	20.89	63.29	0.52
$2Fe_2O_3$	4.18	10.64	17.62	66.94	0.62
1ZnO	4.73	10.64	26.52	57.54	0.58
2ZnO	3.83	9.06	27.29	59.59	0.43
1FeO	3.64	10.56	30.24	53.90	1.66
2FeO	6.06	13.73	25.36	53.45	1.40

and simplify its silicate structural units [22]. In addition, compared with the samples containing ZnO and FeO, the sample containing Fe_2O_3 had a relatively higher Q^3Si content, which represented a higher degree of silicate network connectivity.

Fig. 4 shows the Raman spectra of the spinel in the glass matrix. The spinel's point group is *Fd3m* and usually has the following vibration modes: $A_{1g}(R)+E_g(R)+F_{1g}(R)+3F_{2g}(R)+2A_{2u}+2E_u+4F_{1u}(IR)+2F_{2u}$ [23]. There are usually five vibration modes with Raman activity, namely $A_{1g}(R)$, $E_g(R)$, and $3F_{2g}(R)$. According to previous studies on the Raman spectra of the spinel, the peak at 690 cm^{-1} represents tetrahedral stretching vibration of $A_{1g}(R)$, while the peak in the range 530-550 cm^{-1} represents octahedral cation vibration of F_{2g} [24–25]. The results showed that the relative peak intensity of $A_{1g}(R)$ of the ZnO-doping sample was higher, indicating that Zn^{2+} ion occupied a tetrahedral position in the spinel structure. In addition, compared with the samples containing Fe_2O_3 and FeO, the Fe_2O_3-doping sample had a higher relative intensity of F_{2g}, clarifying that Fe element occupied a more octahedral position of the spinel structure. Overall, the addition of oxide affected both the formation of preliminary spinel and the relative content of the structural units in the glass matrix.

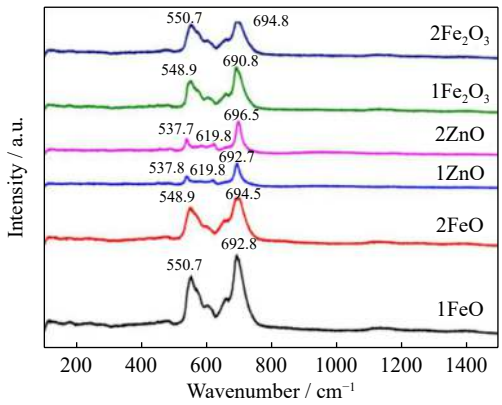

Fig. 4. Raman spectra of the spinel in the parent glass.

3.2. Effect of oxides on the crystallisation thermodynamics of the parent glass

Fig. 5 and Table 5 show the thermal analysis of the parent glass at a heating rate of 10°C/min (T_g: glass transition temperature; T_p: crystallisation temperature). With the addition of Fe_2O_3, nucleation and crystallisation temperatures increased significantly, which might be due to the reduction of mass transfer rate. On the contrary, with the addition of FeO and ZnO, the nucleation temperatures decreased to some extent, indicating that the nucleation temperature was influenced by the polymerisation of silicate network. Moreover, the sample added with 2wt% FeO had the lowest crystallisation temperature, demonstrating the optimum crystallisation condition.

The thermal analysis curves at different heating rates and calculation results are shown in Fig. 5 and Table 6, respectively. In many previous studies, the activation energy of crystallisation reflects the complexity of crystallization. To further research the effect of oxides on crystallisation thermodynamics, the activation energy E_c was calculated using the Kissinger equation with the data of the crystallisation temperatures at different heating rates, which was represented by the following equation [26–29]:

$$\ln\frac{\theta}{T_p^2} = -\frac{E_c}{RT_p} + C \tag{5}$$

where θ represents the heating rate, T_p represents the crystallisation temperature, R represents the gas constant, E_c represents the crystallisation activation energy, and C is a constant. The slope of the curve (X: $-\frac{1}{RT_p}$; Y: $\ln\frac{\theta}{T_p^2}$) after fitting is the crystallisation activation energy.

Compared with previous calculated activation energy of the same matrix composition (429 kJ/mol) [12], the results showed that the activation energy of crystallisation increased with the addition of Fe_2O_3, and decreased with the addition of FeO and ZnO. In general, heterogeneous nucleating agents have two effects on the glass matrix: providing an interface for crystal growth and reducing crystallisation activation energy, and hindering the mass transfer of the melt and increasing the crystallisation activation energy. In the Fe_2O_3-doping sample, a large amount of spinel and Q^3Si units were generated, which affected the efficiency of mass transfer, thus increasing the activation energy to a certain extent. In addition, the sample added with 1wt% Fe_2O_3 had the lowest crystallisation activation energy (388.6 kJ/mol), which indicated that the formation of a certain amount of spinel in the parent glass was beneficial for crystallisation.

The Avrami parameter (n) is used to characterise the crystallisation behaviour, which is positively related to the number of crystallisation directions. Generally, the larger n represents the bulk crysatllisation, while the smaller one represents the surface crystallisation. The Avrami parameter of the parent glass can be calculated using the Augis–Bennett equation [30–31]:

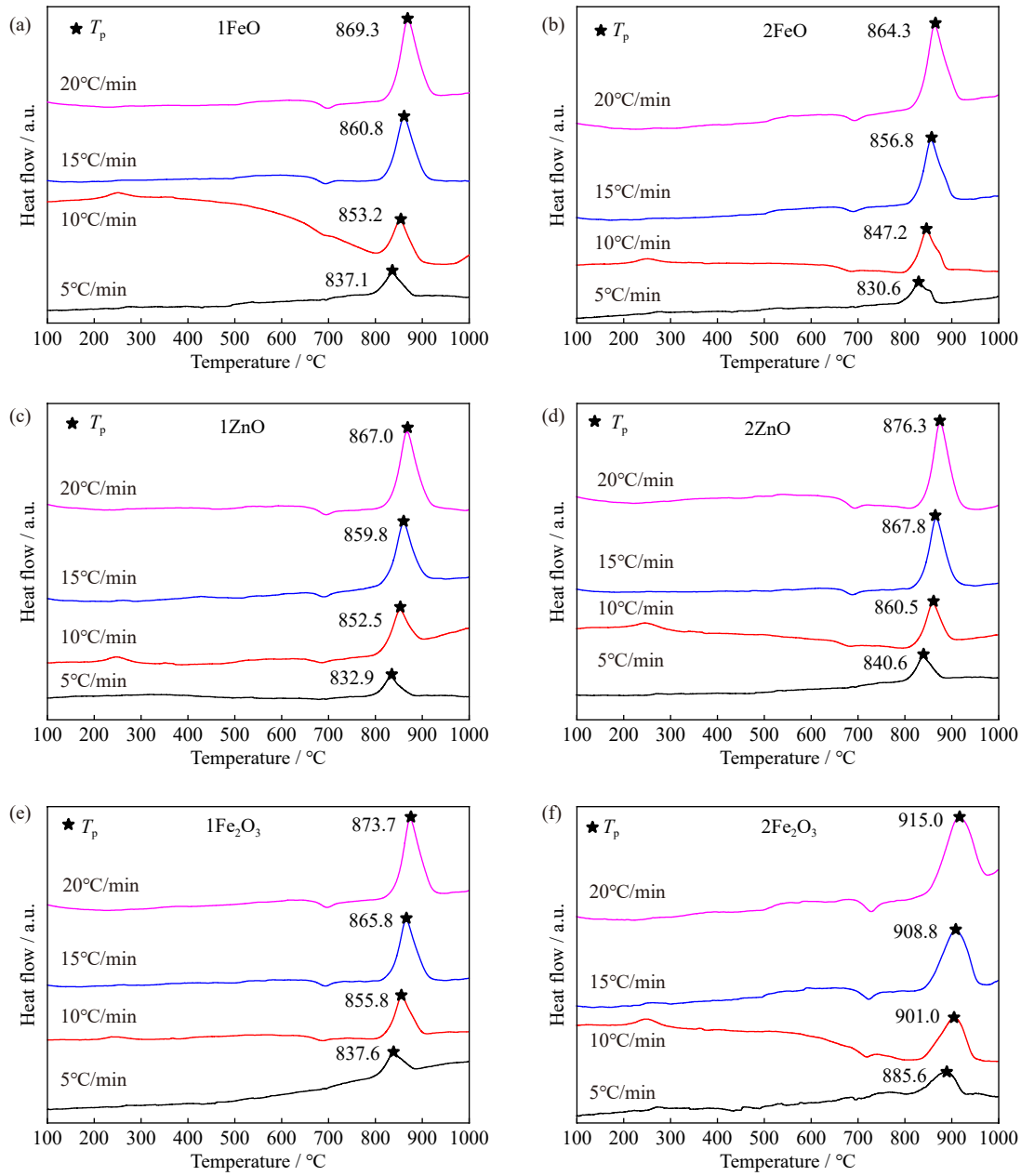

Fig. 5. Thermal analysis of the parent glass (heating rates of 5, 10, 15, and 20°C/min): (a) 1FeO; (b) 2FeO; (c) 1ZnO; (d) 2ZnO; (e) $1Fe_2O_3$; (f) $2Fe_2O_3$.

Table 5. Thermal analysis data of the parent glass (heating rate: 10°C/min) °C

Sample	T_g	T_p
$1Fe_2O_3$	686.5	855.8
$2Fe_2O_3$	718.5	901.0
1ZnO	686.2	852.5
2ZnO	681.2	860.5
1FeO	688.5	853.2
2FeO	682.5	847.2

$$n = \frac{2.5RT_p^2}{\omega E_c} \tag{6}$$

where $\Delta\omega$ is the width of the crystallisation peak at half the height. The results showed that with an increase in the FeO and ZnO content, the Avrami parameters increased. The effect of ZnO was more prominent, indicating that the sample underwent bulk crystallisation. In contrast, the addition of Fe_2O_3 significantly reduced the Avrami parameter, indicating that surface crystallisation was dominant in the 2wt% Fe_2O_3 sample. Otherwise, compared with n of previous study [12,32], its value of all samples decreased to some extent. This may be caused by the foramtion of spinel and the consumption of network modifiers (MgO). Overall, ZnO-doping samples displayed better crystallisation thermodynamic conditions.

3.3. Effect of oxides on the crystal growth and microstructure of the glass ceramics

Fig. 6 shows the XRD diffraction peaks of the glass

Table 6. Thermal analysis data and calculation results of the parent glass

Sample	Crystallisation temperature / °C				E_c / (kJ·mol^{-1})	Avrami parameter, n
	5°C/min	10°C/min	15°C/min	20°C/min		
1FeO	837.1	853.2	860.8	869.3	442.6	1.459
2FeO	830.6	847.2	856.8	864.3	410.0	1.562
1ZnO	832.9	852.5	859.8	867.0	408.6	1.653
2ZnO	840.6	860.5	867.8	876.3	399.7	1.908
1Fe_2O_3	837.6	855.8	865.8	873.7	388.6	1.715
2Fe_2O_3	885.6	901.0	908.8	915.0	521.8	0.839

ceramics. The results showed that the main crystal phase of all samples was augite with a high degree of crystallisation. Augite is a chain silicate with the chemical formula: $Ca(Mg,Fe,A1)(Si,A1)_2O_6$ in which Ca, Mg elements occupy the octahedral coordination, and Si–O tetrahedrons form a long chain.

The cell parameters calculated by Rietveld refinement using FullProf software are listed in Table 7. The results showed that the cell parameters a and β of the augite phase in all samples increased to a certain extent compared with the CIF data ($CaMg_{0.7}Al_{0.6}Si1_{.7}O_6$). With an increase in the Fe_2O_3 content, a decrease in the parameters was observed. Compared with sample 1ZnO, the cell parameter a of sample 2ZnO increased. The cell parameter b of sample 2FeO was bigger than that of sample 1FeO. This phenomenon was attributed to the participation of Fe^{3+}, Fe^{2+}, and Zn^{2+} ions in augite phase. Fe^{3+} with small radius, and Fe^{2+} and Zn^{2+} with large radius replaced the positions of Ca^{2+} and Mg^{2+} ions to form a solid structure.

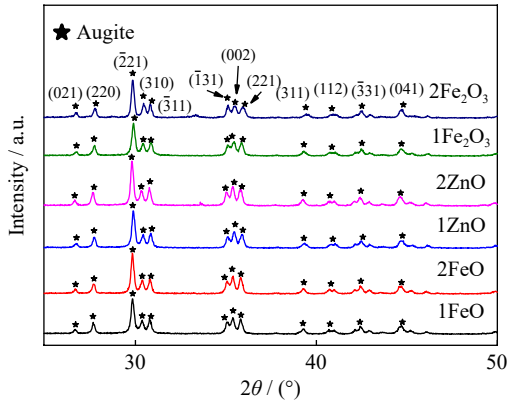

Fig. 6. XRD patterns of the glass ceramic samples.

Furthermore, the addition of oxides changed the relative intensity of the diffraction peaks. The addition of Fe_2O_3 reduced the intensity of diffraction peaks at about 30.914°, 35.466°, and 35.809°, ZnO increased and decreased the peak at 30.419° and 35.266°, respectively, and FeO enhanced the peak at 29.895°. These results indicated that oxides had a varying influence on the relative quantities of augite crystal planes. The effect of Fe_2O_3 was more significant, which was consistent with the change reflected by cell parameters.

Fig. 7 shows the microstructure of the heat-treated glass ceramics. With the addition of FeO, Fe_2O_3, and ZnO, the grains of augite phase were refined. The size ranges of the augite were 7.438–10.181 μm (1FeO), 3.868–6.655 μm (2FeO), 5.857–7.652 μm (1ZnO), 5.199–6.432 μm (2ZnO), 7.186–19.362 μm (1Fe_2O_3), and 5.099–8.387 μm (2Fe_2O_3), which showed that ZnO promoted the uniform growth of augite. Otherwise, the spinel size of the Fe_2O_3-doping sample was larger than those of the others, and the phenomenon of spinel aggregation demonstrated an uneven distribution. By comparison, spinel with finer size was evenly distributed in the ZnO and FeO-doping samples. The sample added with 2wt% ZnO had a denser and more regular microstructure.

Table 8 lists the EPMA data of glass ceramics. Compared with the results of the parent glass (Table 3), the data indicated that after the heat treatment, Fe^{2+}, Fe^{3+}, and Zn^{2+} in the matrix were more inclined to participate in the formation of spinel. The results also showed that most of Zn element was enriched in the spinel phase, while its content in the augite phase was relatively small. In addition, due to the influence of Zn^{2+}, the content of Cr^{3+} in the glass matrix and augite phase was relatively low, which indicated that the addition of Zn^{2+} can effectively promote the enrichment of Cr^{3+} in the spinel phase.

Table 7. Unit cell parameters of PDF card and samples

Sample	Axis / nm			Axial angle / (°)		
	a	b	c	α	β	γ
CIF data	0.9717	0.8886	0.5288	90	106.29	90
1FeO	0.974409	0.886371	0.528271	90	106.3300	90
2FeO	0.974095	0.886669	0.528336	90	106.3521	90
1ZnO	0.974175	0.886984	0.527870	90	106.3606	90
2ZnO	0.974344	0.886780	0.527867	90	106.3367	90
1Fe_2O_3	0.974230	0.886845	0.528166	90	106.3096	90
2Fe_2O_3	0.972043	0.885242	0.527523	90	106.6071	90

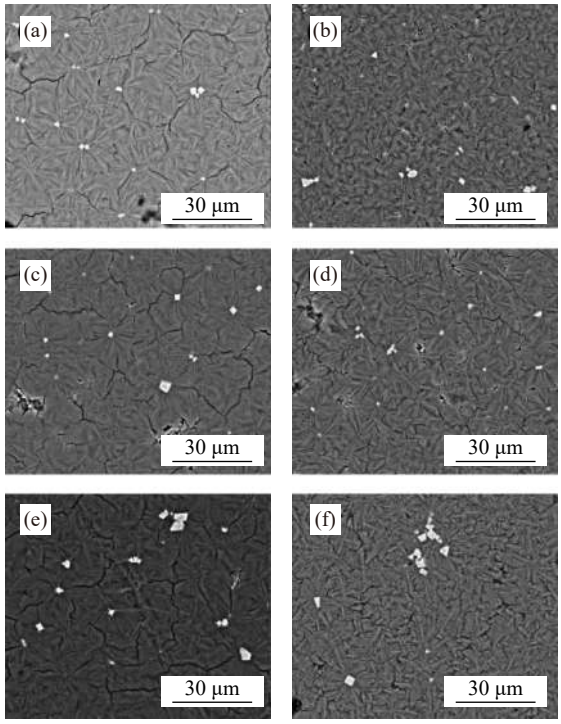

Fig. 7. Microstructures of glass ceramics: (a) 1FeO; (b) 2FeO; (c) 1ZnO; (d) 2ZnO; (e) $1Fe_2O_3$; (f) $2Fe_2O_3$.

3.4. Effect of oxides on physical and chemical properties of glass ceramics

Table 9 lists the physicochemical properties of glass ceramics. With an increase in the oxide content, the density of the sample was observed to increase. In terms of mechanical properties, the addition of FeO reduced the flexural strength of the material, while ZnO and Fe_2O_3 improved it. The 2wt% ZnO-doping sample displayed the maximum flexural strength (170.3 MPa), indicating that ZnO played a significant role in the structural reinforcement. All the samples displayed good chemical stability. Except for the 1wt% FeO-doping sample, the acid and alkali resistance of all the samples were more than 99.9wt%. In addition, the results also showed that the sample containing 2wt% Fe_2O_3 had the strongest chemical corrosion resistance, and previous studies also confirmed this conclusion [33]. In terms of material safety, chromium leaching concentrations of all samples were less than the national standard (1.5 mg/L), while the 2ZnO and $2Fe_2O_3$ samples had better chromium solidification ability. All the products were environmentally friendly and can be used as artificial stones.

Combined with above research, it was determined that a proper amount of ZnO can be added to the melt for the preparation of glass ceramics, which can effectively improve the thermodynamic conditions of crystallisation, while enhancing the physical and chemical properties of the prepared materials and solidification ability of chromium. Therefore, adding appropriate amounts of zinc-containing dust and sludge into raw materials can effectively utilise this part of resources and solidify the heavy metal elements into a crystal structure. However, FeO and Fe_2O_3 have negative effects on the preparation of glass ceramics in some respects, so the dosage of Fe-containing raw material needs to be strictly limited.

Table 8. EPMA quantitative analysis of glass ceramics mol%

Sample	Phase	Composition (Relative error)						
		CaO (2%)	MgO (2%)	Al_2O_3 (2%)	SiO_2 (2%)	Cr_2O_3 (2%)	ZnO (5%)	FeO (5%)
1FeO	Augite	19.759	21.814	6.422	50.284	0.269	—	1.452
	Spinel	1.248	46.434	6.587	0.661	40.408	—	4.663
2FeO	Augite	19.717	21.446	6.101	49.530	0.280	—	2.926
	Spinel	1.165	42.398	5.941	0.405	39.880	—	10.207
1ZnO	Augite	19.380	22.256	6.341	51.319	0.219	0.484	—
	Spinel	2.211	38.582	6.538	3.830	42.371	6.468	—
2ZnO	Augite	19.517	22.750	6.349	50.496	0.198	0.692	—
	Spinel	1.339	32.914	7.192	2.291	44.942	11.325	—
$1Fe_2O_3$	Augite	19.204	21.573	6.585	51.384	0.215	—	1.040
	Spinel	2.744	44.877	6.202	4.568	38.218	—	3.392
$2Fe_2O_3$	Augite	20.217	22.271	6.625	48.472	0.320	—	2.101
	Spinel	1.966	41.968	6.211	1.771	41.292	—	7.127

Table 9. Physicochemical properties of glass ceramics

Sample	Density / ($g \cdot cm^{-3}$)	Flexural strength (±2%) / MPa	Acid resistance / %	Alkali resistance / %	Total leached Cr concentration / ($mg \cdot L^{-1}$)
1FeO	2.947	145.1	99.844	99.926	0.561
2FeO	2.989	126.9	99.956	99.955	0.863
1ZnO	2.948	101.1	99.958	99.960	0.727
2ZnO	3.003	170.3	99.951	99.945	0.349
$1Fe_2O_3$	2.977	122.5	99.919	99.951	0.342
$2Fe_2O_3$	3.085	134.3	99.986	99.984	0.309

4. Conclusions

(1) Oxides resulted in many preliminary spinels in the glass matrix. FeO, ZnO, and Fe_2O_3 played a prominent role in the formation of spinel, while FeO influenced the structure of the parent glass and simplified the silicate network.

(2) The activation energy of crystallisation increased with the addition of Fe_2O_3, but decreased with the addition of FeO and ZnO. A small amount of spinel in the parent glass was beneficial for promoting crystallisation. FeO and ZnO promoted the bulk crystallisation of the parent glass.

(3) The main crystal phase of all samples was augite with a high degree of crystallisation. With an increase in the Fe_2O_3 content, a decrease in the cell parameters was observed. On the contrary, ZnO and FeO increased the cell parameters *a* and *b*, respectively. After adding oxides, the grains of augite phase were refined. The relative quantities of augite crystal planes were also influenced. The addition of Zn^{2+} can effectively promote the enrichment of Cr^{3+} in the spinel phase.

(4) With an increase in the oxide content, the density of glass ceramics increased. FeO reduced the flexural strength of the material, while ZnO and Fe_2O_3 increased it. ZnO played a significant role in the structural reinforcement. All the samples displayed good chemical stability. Chromium leaching concentrations of all samples were less than the national standard (1.5 mg/L), which confirmed the safety of the materials. Appropriate amounts of zinc-containing dust and sludge can be used as raw materials in the preparation of glass ceramics.

Acknowledgements

This work was financially supported by the National Key R&D Program of China (No. 2019YFC1905701), the National Natural Science Foundation of China (Nos. U1960201 and 52204336), and the China Postdoctoral Science Foundation (No. 2022M710359).

Conflict of Interest

The authors declare that they have no known competing financial interests or personal relationships that could have appeared to influence the work reported in this paper.

References

[1] A.V. DeCeanne, L.R. Rodrigues, C.J. Wilkinson, J.C. Wilkinson, and E.D. Wilkinson, Examining the role of nucleating agents within glass-ceramic systems, *J. Non-Cryst. Solids.*, 591(2022), p. 121714.

[2] D. He, H. Ma, and H. Zhong, Effect of different nucleating agent ratios on the crystallization and properties of MAS glass ceramics, *J. Eur. Ceram. Soc.*, 41(2021), No. 16, p. 342.

[3] J. Zhong, J. Zhang, Y. Yu, H. Bai, Z. Zhang, and Y. Huang, Transparent $MgO-Al_2O_3-SiO_2$ glass-ceramics prepared with ZrO_2 and SnO_2 as nucleating agents, *J. Non-Cryst. Solids.*, 588(2022), p. 121585.

[4] Z. Luo, H. Liang, C. Qin, T. Liu, and A. Liu, Crystallization kinetics and phase formation of $Li_2O-SiO_2-Si_3N_4$ glass-ceramics with P_2O_5 nucleating agent, *J. Alloys Compd.*, 786(2022), p. 688.

[5] C. Wang, H. Jia, A. Wang, X. Wang, Y. Guo, and J. Zhang, Effect of TiO_2 on the crystallization and properties of $MgO-Al_2O_3-SiO_2$ glass-ceramics prepared by an “one-step" method from laterite ore, *Ceram. Int.*, 45(2019), No. 4, p. 5133.

[6] L. Deng, R. Jia, F. Yun, X. Zhang, H. Li, M. Zhang, X. Jia, D. Ren, and B. Li, Influence of Cr_2O_3 on the viscosity and crystallization behavior of glass ceramics based on blast furnace slag, *Mater. Chem. Phys.*, 240(2020), p. 122212.

[7] Y. Shi, X.W. Song, and X.X. Han, Catalytic mechanism of iron oxide doping on the crystallization process of Cr_2O_3-containg glass ceramics, *J. Non Cryst. Solids.*, 570(2021), p. 121002.

[8] G.S. Back, M.J. Yoon, and W.G. Jung, Effect of the Cr_2O_3 and TiO_2 as nucleating agents in $SiO_2-Al_2O_3-CaO-MgO$ glass-ceramic system, *Met. Mater. Int.*, 23(2017), p. 798.

[9] G.A. Khater, Influence of Cr_2O_3, LiF, CaF_2 and TiO_2 nucleants on the crystallization behavior and microstructure of glass-ceramics based on blast-furnace slag, *Ceram. Int.*, 37(2011), No. 7, p. 2193.

[10] S. Zhang, Y.L. Zhang, and Z.M. Qu, Effect of soluble Cr_2O_3 on the silicate network, crystallization kinetics, mineral phase, microstructure of $CaO–MgO–SiO_2–(Na_2O)$ glass ceramics with different CaO/MgO ratio, *Ceram. Int.*, 45(2019), No. 9, p. 11216.

[11] Y. Shi, B.W. Li, M. Zhao, and M.X. Zhang, Growth of diopside crystals in CMAS glass-ceramics using Cr_2O_3 as a nucleating agent, *J. Am. Ceram. Soc.*, 101(2018), No. 9, p. 3968.

[12] S. Zhang, Y.L. Zhang, J.T. Gao, Z.M. Qu, and Z. Zhang, Effects of Cr_2O_3 and CaF_2 on the structure, crystal growth behavior, and properties of augite-based glass ceramics, *J. Eur. Ceram. Soc.*, 39(2019), No. 14, p. 4283.

[13] M.C. Kemei, P.T. Barton, S.L. Moffitt, *et al.*, Crystal structures of spin-Jahn–Teller-ordered $MgCr_2O_4$ and $ZnCr_2O_4$, *J. Phys.: Condens. Matter*, 25(2013), No. 32, art. No. 326001.

[14] M. Robbins, G.K. Wertheim, R.C. Sherwood, and D.N.E. Buchanan, Magnetic properties and site distributions in the system $FeCr_2O_4–Fe_3O_4(Fe^{2+}Cr_{2-x}Fe^{3+}_xO_4)$, *J. Phys. Chem. Solids*, 32(1971), No. 3, p. 717.

[15] M.Z. Zhao, J.W. Cao, Z. Wang, and G.H. Li, Precipitating spinel into precursor glass and its assistance in crystallization, *J. Eur. Ceram. Soc.*, 39(2019), No. 7, p. 2427.

[16] J.L. Li, A.J. Xu, D.F. He, Q.X. Yang, and N.Y. Tian, Effect of FeO on the formation of spinel phases and chromium distribution in the $CaO–SiO_2–MgO–Al_2O_3–Cr_2O_3$ system, *Int. J. Miner. Metall. Mater.*, 20(2013), No. 3, p. 253.

[17] T. Wu, Y. Zhang, F. Yuan, and Z. An, Effects of the Cr_2O_3 content on the viscosity of $CaO–SiO_2–10$ Pct $Al_2O_3–Cr_2O_3$ quaternary slag, *Metall. Mater. Trans. B.*, 49(2018), p. 1719.

[18] Q. Li, J. Gao, Y. Zhang, Z. An, and Z. Guo, Viscosity measurement and structure analysis of Cr_2O_3-bearing $CaO–SiO_2–MgO–Al_2O_3$ slags, *Metall. Mater. Trans. B.*, 48(2017), p. 346.

[19] Q. Li, S. Yang, Y. Zhang, Z. An, and Z. Guo, Effects of MgO, Na_2O, and B_2O_3 on the viscosity and structure of Cr_2O_3-bearing $CaO–SiO_2–Al_2O_3$ slags, *ISIJ. Int.*, 57(2017), No. 4, p. 689.

[20] S. Zhang, Y. Zhang, S. Wu, Z. Zhao, and Y. Wu, Long-term leaching mechanism of chromium-containing slag after vitrification and heat treatment, *Ceram. Int.*, 48(2022), No. 9, p. 13366.

[21] F. Yuan, Z. Yuan, Y. Zhang, and T. Wu, Effect of Al_2O_3 content on the viscosity and structure of $CaO–SiO_2–Cr_2O_3–Al_2O_3$ slags, *Int. J. Miner. Metall. Mater.*, 29(2022), No. 8, p. 1522.

[22] Y.S. Lee, D.J. Min, S.M. Jung, and S.H. Yi, Influence of basicity and FeO content on viscosity of blast furnace type slags containing FeO, *ISIJ Int.*, 44(2004), No. 8, p. 1283.

[23] Z.W. Wang, P. Lazor, S.K. Saxena, and G. Artioli, High-pres-

sure Raman spectroscopic study of spinel ($ZnCr_2O_4$), *J. Solid State Chem.*, 165(2002), No. 1, p. 165.

[24] W.J. Yong, S. Botis, S.R. Shieh, W.G. Shi, and A.C. Withers, Pressure-induced phase transition study of magnesiochromite ($MgCr_2O_4$) by Raman spectroscopy and X-ray diffraction, *Phys. Earth Planet. Inter.*, 196-197(2012), p. 75.

[25] K.F. McCarty and D.R. Boehme, A Raman study of the systems $Fe_{3-x}Cr_xO_4$ and $Fe_{2-x}Cr_xO_3$, *J. Solid State Chem.*, 79(1989), No. 1, p. 19.

[26] W. Li, C. Deng, Y. Chen, X. Wang, C. Yu, J. Ding, and H. Zhu, Application of Cr_3C_2/C composite powders synthesized via molten-salt method in low-carbon MgO−C refractories, *Ceram. Int.*, 48(2022), No. 11, p. 15227.

[27] J. Yang, B. Liu, S.G. Zhang, and A.A. Volinsky, Glass-ceramics one-step crystallization accomplished by building Ca^{2+} and Mg^{2+} fast diffusion layer around diopside crystal, *J. Alloys Compd.*, 688(2016), p. 709.

[28] N. Saheb, S. Lamara, F. Lamara, and S.F. Hassan, Kinetics of α-cordierite formation from nano-oxide powders, *Ceram. Int.*, 48(2022), No. 16, p. 23921.

[29] Y. Li, D. Cao, Y. Zhang, and X. Jia, Performance of a dry-method-epoxy modifier and a modified epoxy-asphalt mixture, *Constr. Build. Mater.*, 266(2021), p. 120229.

[30] J.A. Augis and J.E. Bennett, Calculation of the Avrami parameters for heterogeneous solid state reactions using a modification of the Kissinger method, *J. Therm. Anal.*, 13(1978), No. 2, p. 283.

[31] A. Karamanov and M. Pelino, Crystallization phenomena in iron-rich glasses, *J. Non Cryst. Solids*, 281(2001), No. 1-3, p. 139.

[32] M.R. Boudchicha, F. Rubio, and S. Achour, Synthesis of glass ceramics from Kaolin and dolomite mixture, *Int. J. Miner. Metall. Mater.*, 24(2017), No. 2, p. 194.

[33] H.P. Liu, X.F. Huang, L.P. Ma, D.L. Chen, Z.B. Shang, and M. Jiang, Effect of Fe_2O_3 on the crystallization behavior of glass-ceramics produced from naturally cooled yellow phosphorus furnace slag, *Int. J. Miner. Metall. Mater.*, 24(2017), No. 3, p. 316.